Journal of Energy Challenges and Mechanics
http://www.nscj.co.uk/JECM/
ISSN 2056-9386
Volume 3 (2016) issue 1, article 3

Time varying waveform distortions caused by dispersed generators in Smart Grids

由智能电网中分散发电机所导致的随时间变化之波形失真

L. Alfieri[1*], A. Bracale[2]

[1]*Department of Electrical Engineering and of Information Technology, University of Naples Federico II, Naples - 80125, Italy*
[2]*Department of Engineering, University of Naples Parthenope, Naples - 80143, Italy*

luisa.alfieri@unina.it

Accepted for publication on 12th October 2015

Abstract - **Among power quality disturbances, the distortions of voltage and current waveforms are turning into one of the most important issues, due to the great diffusion of electronic power converters used to supply loads or interconnect the distributed energy resources (DER) to the grid. In particular, wind turbines systems (WTS) and photovoltaic systems (PVS) are the most extensively used DER in the actual active distribution networks, and these systems are expected to rise fast in the future smart grids (SGs) as a result from the forecasted economic advantages. This paper provides a review of the theoretical aspects about the most common PVS and WTS configurations and about the waveform distortions introduced by both these systems at the point of common coupling in several operating conditions. Numerical applications are also performed by applying an advanced spectral analysis method which seems particularly suitable to capture the time-varying nature of the current and voltage waveforms of the systems under study.**

Keywords - **Smart grid, power quality, waveform distortions, wind turbine systems, photovoltaic systems.**

I. INTRODUCTION

Currently, the interest towards the Power Quality (PQ) disturbances is growing since adequate PQ levels guarantee the necessary compatibility between all of the equipment connected to the grid. In particular, in the smart grids (SGs) context, the distortions of voltage and current waveforms are turning into one of the most important issue, due to the great diffusion of the electronic power converters to supply loads or to interconnect the distributed energy resources (DER) to the grid [1-4].

Indeed, the widespread use of DER in SGs contributes significantly to the waveform distortions which can be not acceptable for sensitive loads. In particular, wind turbines systems (WTS) and photovoltaic systems (PVS) are the most extensively used DERs in the actual distribution networks, and these systems are expected to rise fast in the future SGs, as a result from the forecasted reduction in investment costs and to other economic incentives.

Different configurations are available to connect WTSs and PVSs to the grid; each of them can generate time-varying voltage and current waveform distortions characterized by spectral components at low and high frequencies, which can reach significant magnitudes in specific operating conditions [3-4]. Therefore, the study of their impact on the distribution networks is a topic of great interest and widely discussed in the relevant literature [5].

Motivated by the aforesaid considerations, the main objective of this paper is to provide an overview of the most common PVS and WTS configurations and of the waveform distortions introduced by these systems at the point of common coupling (PCC) in several operating conditions [6-16].

The theoretical aspects of the problems are enriched by numerical applications on actual current waveforms. The numerical experiments are performed by applying the advanced spectral analysis method proposed in [17], based on modifications of the ESPRIT signal models; this method was proved to be particularly suitable to capture the time-varying nature of the current and voltage waveforms introduced by the

©2015 North Sea

systems which are aim of our study, also requiring a reduced computational effort.

This paper is organized as follows. Section II briefly describes the different PVS and WTS schemes, discussing the typical waveform distortions caused by each of these systems. In Section III the advanced method proposed in [17] is briefly recalled and in Section IV numerical experiments are shown, comparing the spectra obtained by using the proposed method with the spectra that are theoretically expected. Conclusions are presented in Section V.

II. WAVEFORM DISTORTION IN THE MOST COMMON SCHEME OF PV AND WT SYSTEMS

It is well known that active distribution networks are experiencing the widespread use of DERs and that the most diffuse sources of renewable energy are solar and wind plants. In this section, an overview of the most common PVS and WTS schemes is provided, paying particularly attention to the waveform distortions caused by each of them.

In particular, primary and secondary spectral emissions are considered: the first typology refers only to the distinctive disturbances of the considered system; the second typology of emissions refers to the disturbances caused by other sources near the system (i.e., non-linear loads and power communication signals) [14].

Moreover, the spectra of voltage and current waveforms at the PCC of both PVSs and WTSs include a wide range of frequencies. For the sake of clarity, in the following, the spectral components are classified as "low-frequency components" (up to 2 kHz) and "high-frequency components" (over 2 kHz).

2.1. PHOTOVOLTAIC SYSTEM

A PVS is connected to the grid through inverters, that, basically, realize the DC/AC conversion of the electric energy, fulfilling particular specifications in terms voltage and frequency. The photovoltaic inverters are among the most advanced electronic power converters, since they are controlled in order to perform important tasks, such as the maximum power point tracking, the anti-islanding and the grid synchronization; therefore their functionalities must be improved with respect, for instance, to motor drive inverters, and this fact influences their hardware complexity [6,13, 18].

Based on the typologies of the inverters used, the PVSs assume different characteristics and benefits, i.e., the large-scale PVSs can be connected to the grid through a three-phase inverter or through three single-phase inverters combined as a "quasi three-phase" inverter. In the first case, no zero-sequence emissions are found in the waveform spectra and the load balancing among the phases is guaranteed, but its efficiency and reliability are poorer than those of the latter solution. In addition, since the large-scale photovoltaic plants could be expanded over time, single-phase inverters prove to be more versatile than three-phase inverters, in order to guarantee an easier spread of the system. In this context, hybrid configurations, such as the multi-string inverters, can be useful to obtain the combined benefits of the previous configurations [15].

The inverter is the core element of the whole PVS, highly influencing the system efficiency, lifetime and size; many research activities focused on its improvement and development, making available a large variety of photovoltaic inverters. Fig. 1 shows the schemes of PVSs connected through (i) inverters with line frequency isolation transformers (Fig. 1a), (ii) inverters with high frequency isolation transformers (Fig. 1b), and (iii) inverters without isolation transformers (Fig. 1c). These are among the most common solutions for the PVSs, and each of them is able to satisfy particular requirements [6, 15].

The first two solutions are suitable when galvanic isolation and voltage step-up are required for the system. The solutions with line frequency transformers provide higher efficiency than those with high frequency transformers, since they need less power stages than the latter, but they are also the most expensive configurations. Single-phase PVS connected through both line-frequency and high-frequency transformers are characterized by primary emissions with relevant third harmonic components, introduced by the magnetizing currents of the transformers. The magnitude of these components significantly increase when the transformer operates over the rated voltage, since, in these operating conditions, the magnetizing currents increase [18, 19].

When the galvanic isolation is not required, an inverter without isolation transformer can be used; it guarantees both economic efficiency and high performances, with primary emissions introduced only by the particular PWM technique used for the inverter control [18, 20].

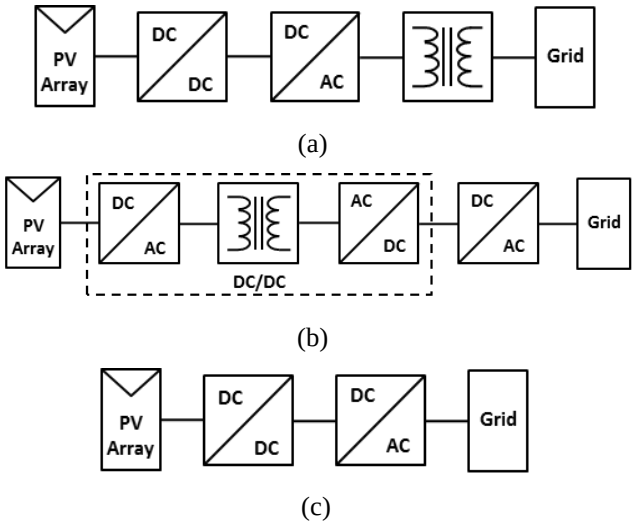

Fig. 1, Schemes of single-phase PVSs: (a) inverter with line-frequency isolation transformer; (b) inverter with high-frequency isolation transformer; (c) inverter without an isolation transformer.

However, different operating conditions of the PVS cause different waveform distortions, which are generally reduced by the presence of the LC filters. Note that the harmonics and interharmonics usually do not change significantly as the PV power changes; however, some harmonics could slightly

increase as the power increases, and the use of multiple inverters in a PVS produces usually lower levels of emissions than the use of an unique, large-size inverter [21].

In particular, in [22] the behavior of the distorting spectral components at the PCC in a 800 kWp-PV plant was analyzed; the PV system is constituted by 16 three-phase inverters and the analysis was performed for two intervals of active power equal to 0÷10% and 90÷100% of rated power respectively. The results showed that for the low-power interval the distortion level was significantly more relevant than for the high-power interval, and the maximum harmonic current levels established according to the IEC standards were overcome in the first scenario [23-24]. However, in both cases only the spectrum up to 50th harmonic was examined, and significant spectral components were detected in correspondence of the 3rd, 5th, 7th and 11th harmonics, and the effects of a parallel resonance were observed over the 20th harmonic, since high values of amplitude were identified. The authors did not provide any information about which specific low-frequency component was due to PWM over-modulation or to background voltages; they only provided the global incidence of the single PVS on the background harmonics at the PCC through the site total harmonic distortion 95% percentile variation ($STHD_{Uj,95}$). Specifically, this index has been estimated equal to 40.12% in the low-power range and equal to 5.18% in the high-power range, suggesting that the background voltages are the main cause of the low-frequency components.

In general, the PVSs spectral emissions at the PCC can include both low- and high-frequency spectral components. The first typology is due to background distortions (secondary emission) or PWM over-modulation of the inverter (primary emission); the amplitudes of low-frequency components in a single photovoltaic plant in rated conditions generally determine a current total harmonic distortion (THDi) lower than 10%; in resonance conditions, significant voltage distortions can be produced, causing heavy problems for the electric network [15].

High-frequency components are mainly due to the PVS inverter and to its particular PWM technique (primary emission). As shown in [25], these high-frequency components are always detected during the hours of power production of the system while, during the night, the inverter is practically turned off and these components disappear. Basically, these components are mostly harmonics and they appear in correspondence of sideband, centered around integer multiples of the inverter switching frequency. Since for commercially-available inverters the switching frequency usually falls in the range [10÷20] kHz, the spectral components introduced by the inverter belong to the supraharmonics category, for which adequate standards are still aims of study of recent research activities [14, 15, 26].

Also high-frequency secondary emissions can be expected: these are due to background voltage and could increase significantly in presence of series resonance effects.

2.2. Wind Turbine System

A WTS is basically constituted by a mechanical part and by an electrical part: the first converts the kinetic energy of the wind into mechanical energy, yielding the rotation of a motor shaft; the second part produces electrical energy with characteristics proper to feed the grid [18].

Consistent with the great gamma of WTSs available in commerce, different classifications, based upon both the mechanical and electrical part, can be made: i.e., it is possible to find WTSs with different numbers of blades, with different directions of the rotor axis, or with different speed characteristics. This last classification is the most interesting and includes (Fig. 2): (i) fixed-speed wind turbine systems (Fig. 2a), (ii) semi-variable-speed wind turbine systems with a rotor resistance converter (Fig. 2b), (iii) variable-speed wind turbine systems with the doubly fed induction generators (Fig. 2c) and (iv) variable-speed wind turbine systems with full-scale power converters (Fig. 2d) [13, 27, 28]. Each configuration has specific pros and cons and introduces different harmonic and interharmonic waveform distortions.

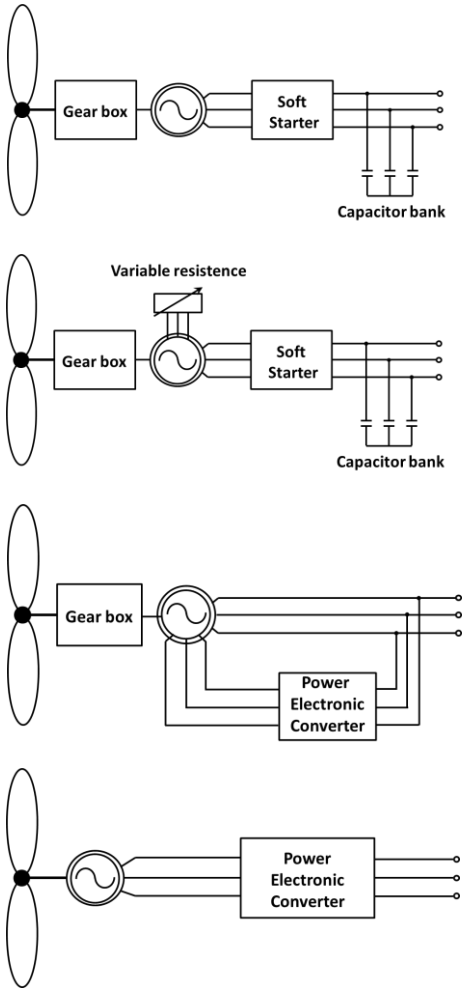

Fig. 2, Schemes of the different Type of WTSs: (a) fixed speed WT; (b) semi variable-speed WT; (c) DFIG WT; (d) full-scale power converter WT.

The first solution (Fig. 2a) is commonly identified as Type-I wind turbine system and it is characterized by the presence of

a gearbox and a squirrel-cage induction generator (SCIG), and by the absence of any power electronic converter. It is linked to the grid by means of a transformer. Generally, this configuration is equipped with an electronic soft-starter, in order to reduce, during the start-up phase, the effect of the in-rush current. Since the SCIG has not an excitation winding, it absorbs reactive power from the network, so a capacitor bank is generally utilized in order to compensate the reactive power [13, 29]. These SCIGs usually work at a nearly-fixed speed, determined mainly by the frequency of the supply grid and by the gear ratio, and it is set above the synchronous speed, according to the SCIG nature. Specifically, since the frequency of the grid is fixed, the only degrees of freedom for the definition of the rotor speed are the gear ratio and the number of poles in the generator. The Type-I wind turbines are cheap and sturdy and they are suitable for a robust frequency control, but they do not guarantee the grid voltage control when an islanding condition occurs; moreover, the wind speed variations are directly turned into electromechanic torque variations, causing mechanical stress [13, 29].

The second configuration (Fig. 2b) is commonly indicated as Type-II wind turbine system and has a structure very similar to the Type-I wind turbines, but it differs for the presence of a wound rotor induction generator (WRIG) with a variable additional rotor resistance, spliced on the rotor shaft and controlled through a converter. Varying this additional resistance, it is possible to control both the power output and the slip of the induction generator, in order to change the rotor speed in a limited range, that is 0÷10% above the synchronous speed [29].

The Type-I and Type-II WTSs are not expected to produce high levels of spectral emissions; therefore, the IEC standards [30] do not specify any particular requirement. However, the action of the soft-starter can produce odd harmonic components at low-frequency, which have low amplitudes and short duration, and triple harmonics can occur in voltage unbalances conditions [31].

The third configuration (Fig. 2c) is commonly identified as Type-III wind turbine system and is characterized by a gearbox and a Doubly Fed Induction Generator (DFIG). Specifically, the stator windings of the generator are directly connected to the grid, while a back-to-back partial-scale static converter is installed between the rotor windings and the grid. This particular allocation of the power electronic converter is the main feature of the scheme, since it allow the rated power of the inverted to be only 30% of the DFIG rated power, although guaranteeing the regulation of the rotor frequency, the regulation of the speed, and the control of active and reactive power. However, the Type-III WTSs have also disadvantages, such as: (i) the presence of a slip ring on the rotor side for the converter connection, (ii) the need of a suitable protection system for the converter when a fault occurs and (iii) the introduction at the PCC of significant waveform distortions, due essentially to the power electronic converter, which impacts on both rotor and stator waveforms [13, 29].

More specifically, the spectral emissions of Type-III WTSs can be classified in inherent components, switching components and spectral components derived by unbalance conditions and by auxiliary loads of the system. The inherent components are related to the not-sinusoidal air gap flux and consist in low-frequency harmonics observable in both current and voltage waveforms. The corresponding frequencies can be evaluated as a function of the actual value of the induction machine slip, s, and of the fundamental frequency f_{fund} of stator voltage as:

$$f_k = |6k(1-s) \pm 1| \cdot f_{fund} \qquad \forall k \in \mathbb{N} \tag{1}$$

The switching components are the most significant components, and they are introduced by the static converter. Specifically, the PWM technique that is used for the control of the converter determines spectral components mainly at high frequency, i.e. around the switching frequency and its multiple, both on the rotor side (and therefore recalled also in the stator side) and on the grid side of the converter. As well known, the frequencies $f_{k,m}^{PWM}$ of the spectral components due to PWM technique, in ideal operative conditions, are given by:

$$f_{k,m}^{PWM} = f_0 + [k \cdot f_{sw} \pm m \cdot f_0] \qquad \forall k \in \mathbb{N}, \forall m \in \mathbb{N}_0 \tag{2}$$

where f_{sw} is the switching frequency, that could be different on the rotor and on the grid side of the converter, and f_0 is: (i) on the grid side, the power system fundamental frequency ($f_0 = f_{fund}$); (ii) on the rotor side, the fundamental frequency of the voltage on that side, which depends on the wind speed and on the gear ratio. The switching components introduced in the rotor side are induced in the stator of the generator, so these components are shifted in frequency at the PCC in dependence on the induction machine slip [13, 32].

When over-modulation conditions occur, also odd low-frequency components are introduced by the PWM technique [13]. The last typology of spectral components introduced at the PCC by the Type-III WTS is due to unbalanced conditions or WTS auxiliary loads (i.e., controllers and motors) [13, 32].

Finally, the forth configuration (Fig. 2d) is identified as Type-IV wind turbine system and is a gearless WTS, characterized by either an induction or a permanent-magnet synchronous generator and a full-scale power electronic converter in cascade. This converter guarantees a self-supporting control of the active/reactive power and the decoupling between the grid and the WTS when a fault occurs, but, on the other hand, the converter cost is higher than the converter used in the Type-III WTS, since, in this configuration, the converter rated power has to be 110% of the rated power of the generator [13, 29].

Even in this configuration, the power electronic converter is the main source of spectral emissions at the PCC, but in this case less spectral components should be detected than in the Type-III wind turbine system, since there is no direct influence through the air gap of the machine. Specifically, in ideal conditions, low-frequency harmonics of order $6k \pm 1$ could be introduced in presence of a six-pulse three-phase bridge rectifier, and therefore a ripple in the DC voltage, in input to

the inverter, could occur [33]. Voltage and current high-frequency components are introduced by the PWM at the PCC, according to eq. (2) with $f_0 = f_{fund}$. Also low-frequency components could be detected, when an over-modulated PWM technique is used [13, 27-28].

Other additional distortions at the PCC of a Type-IV wind turbine system can occur in unbalanced conditions or can be introduced by WTS auxiliary loads [13].

The aforesaid analysis of the waveform distortions introduced by the four typologies of WTSs includes only the primary emission of these systems. However, also secondary emissions are expected at the PCC due to background voltages [13].

III. The Sliding-Window Modified ESPRIT Method

In order to acquire detailed information about the distortion levels caused by actual PVSs and WTSs at the PCC, some PQ indices have been defined in the relevant literature; the evaluation of these indices is conditional to a spectral analysis of the current or voltage waveforms.

The IEC standards recommend, for the spectral analysis, the use of Discrete Fourier Transform (DFT) over successive, rectangular time windows with a fixed duration equal to 10 cycles (12 cycles) of the fundamental period for 50-Hz (60-Hz) systems [34-35]. However, this method is affected by well-known problems, such as the spectral leakage and the fixed frequency resolution, which prevent detailed information on the single spectral components.

In the relevant literature, many spectral analysis methods have been proposed as alternative to the IEC method, in order to overcome the aforesaid problems [36-43]. Among these techniques, reference [17] presented a sliding-window modified ESPRIT method, characterized by both accurate results and reduced computational efforts.

This method is developed by observing that usually the damping factors and the frequencies of spectral components in the power system applications vary slightly versus time, so it is possible to estimate them only a few times, keeping them constant or piecewise constant along the waveform that is analyzed. In particular, the time analysis windows are divided in basis- and no basis-windows, depending on if a traditional ESPRIT algorithm (TEA) or a modified ESPRIT algorithm (MEA) is applied, respectively. In the basis-windows, including the first analysis window, the waveform is analyzed using the traditional ESPRIT model given by:

$$\hat{x}(n) = \sum_{k=1}^{M} A_k e^{j\psi_k} e^{(\alpha_k + j2\pi f_k) n T_s} + r(n), \quad n = 0,1,\dots,N-1 \quad (3)$$

where T_s is the sampling time, M is the number of exponentials, N is the number of samples in the analysis window, $r(n)$ is the added white noise and A_k, ψ_k, f_k, and α_k are the amplitude, the initial phase, the frequency, and the damping factor of the kth complex exponential, respectively; A_k, ψ_k, f_k, and α_k are the unknown parameters of the model. The unknowns are evaluated by solving two equation systems. More in detail: (i) firstly, the eigenvalues $\hat{\lambda}_k^{BW} = e^{\alpha_k^{BW} + j2\pi f_k^{BW}}$ of the rotational matrix are computed, in order to obtain the frequencies and the damping factors; (ii) then, the solution of the equation system constituted by the theoretical definition of the correlation matrix $\boldsymbol{R}_x$ and by the matrix form of eq. (3) is searched with the aim of evaluating the amplitude and the initial phases. In these windows, also the search of the optimal values of the number M of exponentials and of the order N_1 of the correlation matrix is effected; they are updated if the reconstruction error is higher than a pre-fixed threshold. In the no basis-windows, the spectral component parameters $A_k^{BW}, f_k^{BW}, \psi_k^{BW}, \alpha_k^{BW}$ obtained by the basis-window are used in the applied ESPRIT model which is:

$$\hat{x}(n) = \sum_{k=1}^{M} A_k e^{j\psi_k} e^{\left(\alpha_k^{BW} + j2\pi f_k^{BW}\right) n T_s} + r(n) \quad (4)$$

where the only unknown parameters are the amplitudes and the initial phases of the M complex exponentials. It is clear that in these windows the computational burden is less than half of the computational burden required for a basis-window, since only the second equation system has to be solved, and the optimal M and N_1 values do not have to be determined.

Note that, in order to prevent masking effects due to significant variations of frequencies, their evaluation is repeated periodically, generating a new basis-window after a certain number k_f of no basis-windows. The k_f value depends on the particular waveform to be analyzed, and it can be changed dynamically during the analysis, based on different criteria. At each basis-windows, the frequencies and the damping factors are updated and, for the further no basis-windows, the analysis restarts with these new values.

IV. Numerical Applications

The advanced parametric method shown in Section III was used to analyze the waveform distortions due to actual PVSs and WTSs, in order to compare the detected spectral components with the theoretically-expected components.

Several numerical experiments were effected, but for sake of conciseness, only three case studies are reported in this Section. Each of them refers to the analysis of measured current waveforms, and, in particular, the first case study deals with a current recorded at the PCC of a PVS, while, in the second and third case study, a measured current of a Type-I and Type-III wind turbine is analyzed, respectively.

The spectral analysis were performed in MATLAB environment, with programs developed and tested on a Windows PC with an Intel i7-3770 3.4 GHz and 16 GB of RAM.

4.1. Case study 1

Two 1-s current waveforms were recorded at the PCC of a PVS constituted by two 10-kW, three-phase inverter without isolation transformer. The currents were measured on to the same phase of the same inverter and were taken in correspondence of two different levels of produced power: the

first measurement was taken at 8:00 AM, when a low power production was detected; the second measurement was taken at 1:00 PM, when the maximum power supplied in the day was detected. Their time trends are shown in Fig. 3a and Fig. 3b, respectively, and they clearly show different amplitudes and different levels of harmonic and interharmonic.

In both cases the sampling rate was 10 kHz, but a resampling to 20 kHz was performed in order to obtain better performances in the application of the parametric method described in Section III. The reconstruction error threshold for the spectral analysis method was chosen to be equal to 10^{-3}, and the window of analysis is set to slide of 0.04 s.

The spectral analysis revealed mainly the presence of low-frequency spectral components. In fact, although some components were detected in the frequency range 5÷10 kHz, their amplitude was lower than 0.05% of the fundamental amplitude, probably as a consequence of the filter effect; then, they are not reported in the following.

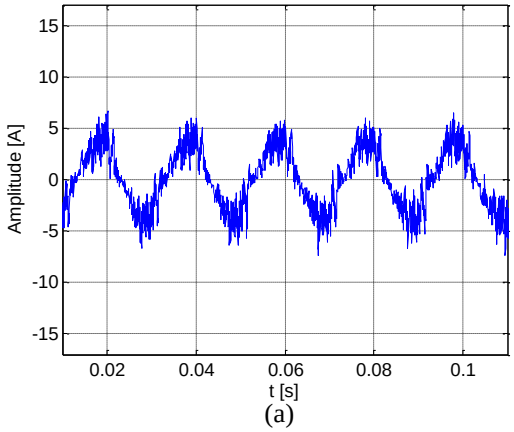

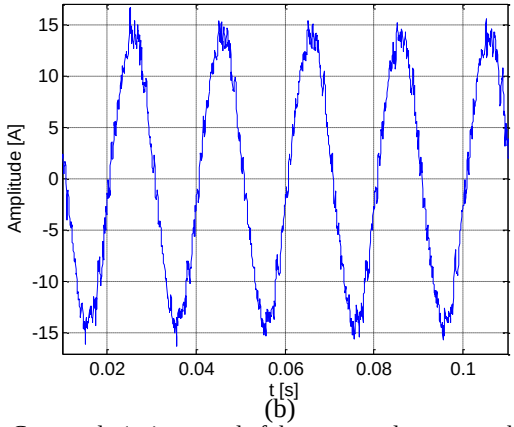

Fig. 3, Case study 1: time trend of the measured current at the PCC of the PVS (a) at the 8:00 AM and (b) at the 1:00 PM.

Fig. 4 shows the spectra obtained by the analysis in the frequency range 0÷5 kHz. Specifically, Fig. 4a shows the spectrum of the current measured at 8:00 AM and Fig. 4b shows the spectrum of the current measured at 1:00 PM. The spectra appear wide and dense in frequency, and, especially for high power production of the system, the amplitudes of both harmonic and interharmonic components have a decreasing trend as the frequency grows. In Fig.4, the fundamental amplitudes both at 8:00 AM and at 1:00 PM are broken off for sake of clearness of the figures; they have a peak value equal to 3.72 A and 13.84 A, respectively. The amplitude scales of the figures were set to magnify all of the other spectral components, that are significantly lower than the fundamental. Coherently with the theoretical expectations, the THD_i of the two currents, evaluated up to 2 kHz, are significantly different; in fact, for the current related to a low level of power production (8:00 AM), the THD_i is about 34%, while, for the current measured at 1:00 PM, the THD_i is slightly higher than 7%. However, comparing the two spectra, it seems that globally the same components are detected, and harmonic and interharmonic amplitudes at 8:00 AM are slightly higher than those observed at 1:00 PM, especially at low-frequency, so the difference in the THDi values is mainly due to the different fundamental amplitude of the two currents.

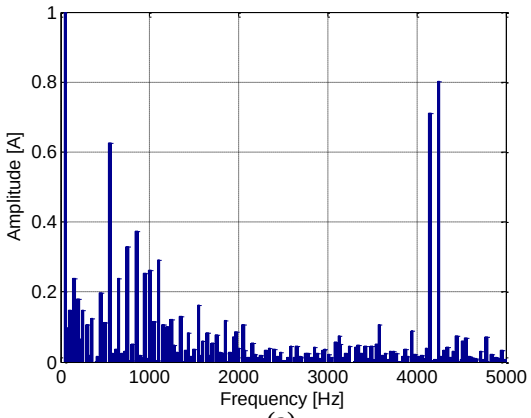

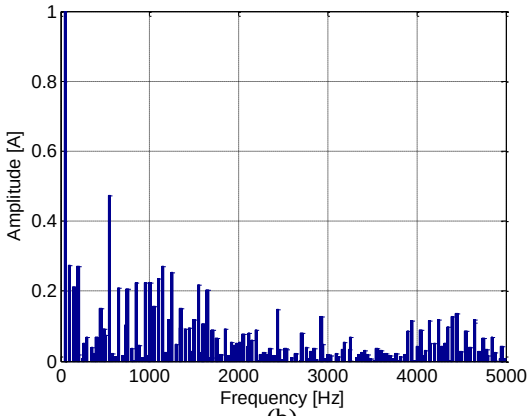

Fig. 4, Case study 1: spectra of the analyzed currents (a) at the 8:00 AM and (b) at the 1:00 PM.

Note that all of the odd and even low-frequency harmonics are detected in both the currents; an investigation on the possible origins of these components was performed. PWM over-modulation is not a suitable cause, since the amplitude modulation ratio is about 0.8. Some components could be introduced by slightly-unbalanced voltage conditions, but in this case the degree of dissymmetry is equal to 1.52%, so the main part of these spectral components probably is due to background voltages.

The presence of two high-frequency components in the sideband centered around 4200 Hz, for the 8:00 AM current, is particularly interesting. The nature of these components is typical of those due to the switching frequency of the inverters, but, since in the current at 1:00 PM their amplitudes decrease, they are probably related to a secondary emission that could be caused by voltage background. In the current at 1:00 PM, other components are detected in the sideband around 2700 Hz. These components appear to be reduced in amplitude in the current at 8:00 AM, so it is possible that are related to a primary emission introduced by the system. Since the aforesaid frequency is incompatible with the common switching frequency, in absence of other information about the system, we could hypothesize that an aliasing phenomenon occurred due to an inadequate sampling rate of the measurements.

4.2. CASE STUDY 2

A 6-s current waveform was recorded during the soft-starting of a Type-I wind turbine. The original sampling rate (2048 Hz) proved to be inadequate for the spectral analysis with the chosen parametric method, so a resampling at 10 kHz was necessary.

For the analysis, the error threshold was set to 10^{-7}, and it was imposed that the window of analysis slid forward by 0.02 s versus time. In Fig. 5a and Fig.5b the time trend of few seconds of this current, and a detail of the same waveform are shown, respectively, in order to point out both its high non-stationary behavior and the typical waveform distortions.

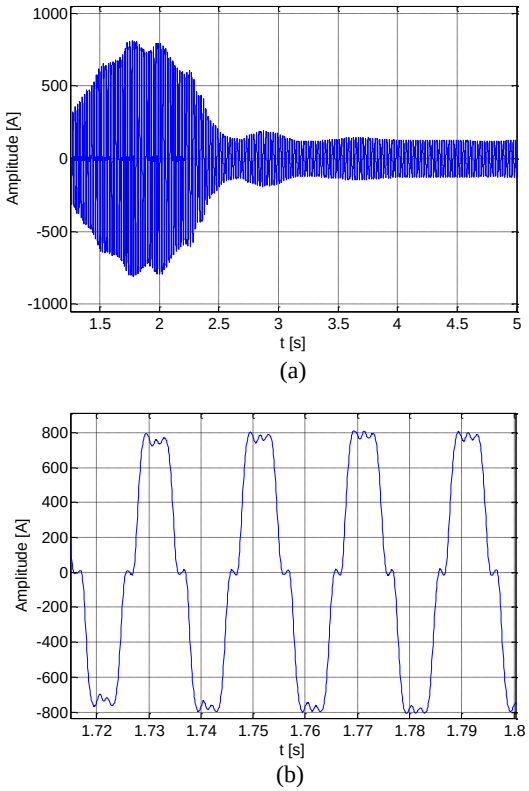

Fig. 5, Case study 2: (a) time trend of the analyzed current; (b) a detail of the same waveform

As expected from the theoretical considerations reported in Section II, the spectral analysis detected that, beyond the fundamental component, also the 3rd, 5th, 7th and 11th harmonic orders had a significant amplitude. Specifically, the time trend of the amplitudes of all of these harmonics appears to increase initially up to a maximum value, and then it decreases until their steady-state value is reached, as shown in Fig. 6, where the time trends of RMS amplitudes of the 5th, 7th and 11th harmonics are provided.

Also in this case, some high-frequency components were detected between 4 kHz and 5 kHz. However, their amplitudes are negligible, being less than 0.03% of the maximum value of the fundamental peak amplitude, that is 864.24A.

4.3. CASE STUDY 3

A 0.2-s current waveform was recorded at the PCC of a Type-III wind turbine. The original sampling rate was 12.8 kHz, so the adopted parametric method was able to detect spectral components in the range of frequency 0÷6400 Hz. The harmonic and interharmonic components appeared severely attenuated as the frequency increases, due to the effect of the filter. In particular, the amplitudes of the components above 3 kHz were lower than 0.04% of the fundamental amplitude, so these components were not dealt with. For the analysis, the error threshold was set to 10^{-5}, and it was imposed that the window of analysis slid forward by 0.01 s versus time. Fig. 7 shows the time trend of the measured current; its stationarity in the time is evident, as well as the reduced waveform distortion. The fundamental component was detected at 50.038 Hz with a peak amplitude of 29.63 A. The other spectral components do not overcame the 1% of the fundamental amplitude, as shown in Fig. 8, where the spectrum obtained by the analysis is reported.

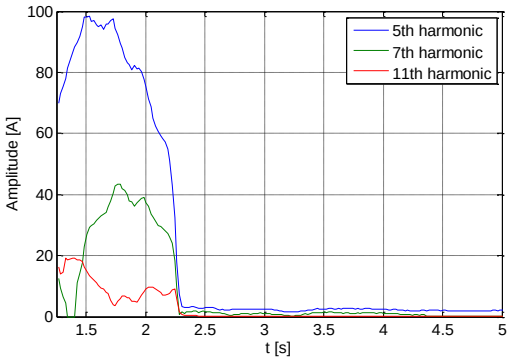

Fig. 6, Case study 2: time trend of the most significant harmonic components

For sake of clearness, the spectrum is divided in two different ranges of frequency: the behavior of the spectrum in the 0÷500 Hz range is shown in Fig. 8a, and the behavior of the spectrum in the 500÷2700 Hz range is shown in Fig. 8b. In both cases, the presence of the inherent components is evident, and they appear to be mainly "twin" interharmonics in correspondence of frequencies that are very close to those expected by applying eq. (1) with similar amplitudes.

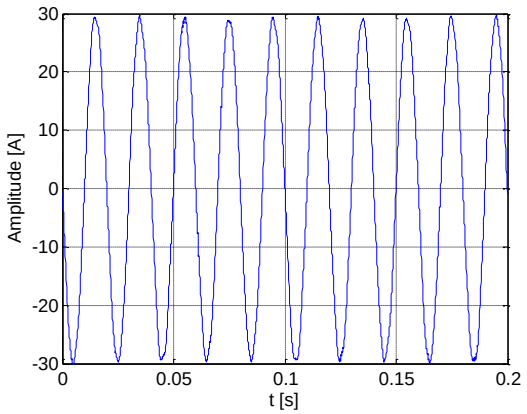

Fig. 7, Case study 3: time trend of the measured current

For example, in Fig. 8a, this behavior can be observed for the interharmonics at 284.94 Hz and at 387.21 Hz, whose amplitudes are equal to 0.28 A and 0.25 A, respectively, and were obtained by eq. (1) for k=1. Similarly, in Fig. 8b, the interharmonics expected for k=2 can be detected at 620.46 Hz and at 717.27 Hz with amplitudes of 0.02 A and of 0.03 A, respectively, and so on.

The harmonics of order 2nd, 3rd, 4th, 5th and 7th also are significant, but their amplitudes are however lower than the first group of inherent components, as shown in Fig. 8a. Finally, Fig. 8b shows that in correspondence of 2.3 kHz there is another significant component, whose amplitude is about 0.24 A. This component could be due to the switching frequency of the static converter on the grid side.

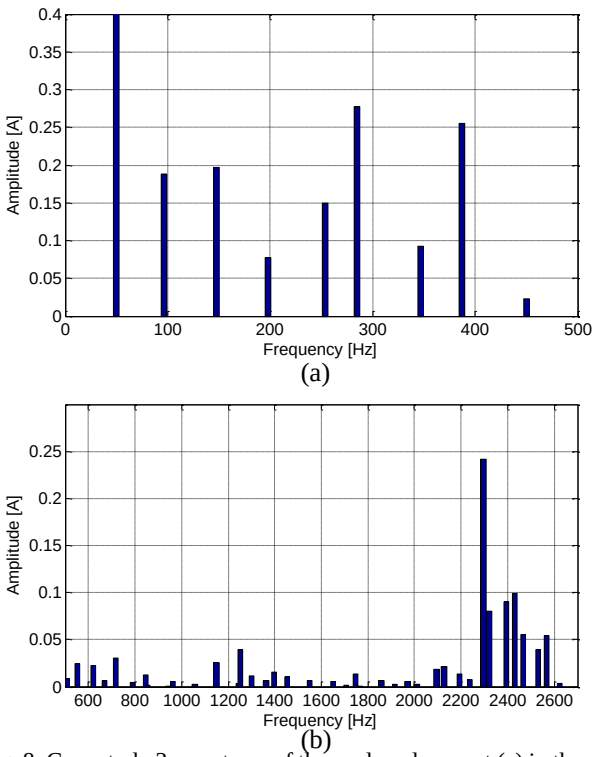

Fig. 8, Case study 3: spectrum of the analyzed current (a) in the range of frequency 0÷500 Hz and (b) in the range of frequency 500÷2700 Hz

V. Conclusions

This paper deals with the waveform distortions caused by the most common PVSs and WTSs. For the different configurations of both systems, a distinction was made among low- and high-frequency spectral emissions, evidencing how the presence of an electronic static converter in the scheme contributes generally to introduce high-frequency disturbance components, and low-frequency spectral components only when over-modulated PWM techniques are used for the control of the converter.

The theoretical discussion was enriched by some numerical applications, where current waveforms measured at the PCC of a PVS and of two different WTS types were analyzed through a modified ESPRIT method. The results of these analyses were proved to be compatible with the theoretical expectances.

Acknowledgement

The authors thank Prof. Guido Carpinelli for his constructive support in the realization of this work.

References

[1] R.H. Lasseter. "Smart Distribution: Coupled Microgrids," *Proceedings of the IEEE* , **99**, pp.1074-1082, 2011

[2] P. Caramia, G. Carpinelli, and P. Verde. *Power Quality Indices in Liberalized Markets.* New Jersey: Wiley-IEEE Press, 2009

[3] F. Blaaiberg, Z. Chen, and S. Baekhoej Kjaer. “Power Electronics as Efficient Interface in Dispersed Power Generation Systems,” *IEEE Trans. on Power Electronics*, **19**, pp. 1184-1194, 2004

[4] R. Angelino, A. Bracale, G. Carpinelli, M. Mangoni, and D. Proto. “Dispersed generation units providing system ancillary services in distribution networks by a centralized control," *IET Renewable Power Generation*, **5**, pp. 311-321, 2011

[5] F. Gronwald. “Frequency versus time domain immunity testing of smart grid components,” *Adv. Radio Sci*, **12**, pp. 149–153, 2014

[6] R.C. Variath, M. A E Andersen, O.N. Nielsen, and A. Hyldgard. "A review of module inverter topologies suitable for photovoltaic systems," *IPEC, 2010 Conference Proc.*, pp. 310-316, 2010

[7] S. A. Papathanassiou, and M. P. Papadopoulos. “Harmonic analysis in a power system with wind generation,” *IEEE Transactions on Power Delivery*, **21**, pp. 2006–2016, 2006

[8] S.T. Tentzerakis, and S.A. Papathanassiou. “An Investigation of the Harmonic Emissions of Wind Turbines,” *IEEE Transactions on Energy Conversion*, **22**, pp. 150-158, 2007

[9] A.E. Feijoo, and J. Cidras. “Modeling of Wind Farms in the Load Flow Analysis,” *IEEE Transactions on Power Systems*, **15**, 2000

[10] J.I. Herrera, T.W. Reddoch, and J.S. Lawler. "Harmonics generated by two variable speed wind generating systems," *IEEE Transactions on Energy Conversion*, **3**, pp. 267–273, 1988

[11] M. H. J. Bollen, and Kai Yang. "Harmonic Aspects of Wind Power Integration

[12] ," *Journal on Modern Power Systems on Clean Energy*, 2013, **1**, pp. 14–21, 2013

[13] *Wind Turbine Generator Systems, Part 21: Measurement and Assessment of Power Quality Characteristics of Grid Connected Wind Turbines*, IEC 61400-21, 2001

[14] L. Alfieri. "Some advanced parametric methods for assessing waveform distortion in a smart grid with renewable generation," *EURASIP Journal on Advances in Signal Processing*, **2015**, pp. 1-16, 2015

[15] S. K. Rönnberg, M. H. Bollen and E. O. A. Larsson. "Emission from small scale PV-installations on the low voltage grid," *Renewable Energy and Power Quality Journal (RE&PQJ)*, 2014

[16] D. Gallo, R. Langella, A. Testa, J.C. Hernandez, I. Papic, B. Blazic, and J. Meyer. "Case studies on large PV plants: Harmonic distortion, unbalance and their effects," *Power and Energy Society General Meeting (PES)*, pp.1-5, July 21--25, 2013

[17] M. H. Bollen and F. Hassan. Integration of Distributed Generation in the Power System. New Jersey: Wiley-IEEE Press, 2011.

[18] L. Alfieri, G. Carpinelli, and A. Bracale. "New ESPRIT-based method for an efficient assessment of waveform distortions in power systems," *Electr Power Syst Res*, **122**, pp. 130–139, 2015.

[19] R. Teodorescu, M. Liserre, and P. Rodriguez. *Grid Converters for Photovoltaic and Wind Power Systems*. New Jersey: Wiley-IEEE, 2011.

[20] J. Zhao, Y. Wang, K. Qu, and F. Li. "Analysis and evaluation of current distortion for photovoltaic system with isolation transformer," *Renewable Power Generation, IET*, **8**, pp. 757-764, 2014

[21] G. Chacko, and R. Scaria. "An Improved Single Phase Transformer less Inverter Topology for Cost Effective PV Systems," *International OPEN ACCESS Journal Of Modern Engineering Research*

[22] S.K. Ronnberg, Kai Yang, M.H.J. Bollen, and A.G.de Castro. "Waveform distortion - a comparison of photovoltaic and wind power," *16th Int. Con. on Harmonics and Quality of Power*, pp. 733-737, May 25--28 May, 2014

[23] M.J. Ortega, J.C. Hernández, and O.G. García. "Measurement and assessment of power quality characteristics for photovoltaic systems: Harmonics, flicker, unbalance, and slow voltage variations," *Electric Power Systems Research*, **96**, pp. 23-35, 2013

[24] *EMC - Part 3-2: Limits – Limits for Harmonic Current Emissions (Equipment Input Current ⩽16A per Phase)*, IEC 61000-3-2, 2009

[25] *EMC – Part 3-12: Limits – Limits for Harmonic Currents Produced by Equipment Connected to Public Low-Voltage Systems with Input Current >16A and ⩽ 75A per Phase*, IEC 61000-3-12, 2004

[26] M. Klatt, A. Dorado, J. Meyer, P. Schegner, J. Backes, and R. Li. "Power Quality Aspects of Rural Grids with High Penetration of Microgeneration, Mainly PV-Installations," *In Proceedings of the 21st International Conference on Electricity Distribution*, Frankfurt, Germany, June 6—9, 2011

[27] N. Mohan, W. P. Robbins, and T. M. Undeland. *Power Electronics: Converters, Applications, and Design*. New Jersey: Wiley, 1995

[28] H. Li, and Z. Chen. "Overview of Different Wind Generator Systems and their Comparisons," *IET Ren. Pow. Gen.*, **2**, pp.123-138, 2008

[29] E. Muljadi, N. Samaan, V. Gevorgian, Jun Li, and S. Pasupulati, "Short Circuit Current Contribution for Different Wind Turbine Generator Types," *IEEE PES General Meeting*, pp. 25-29, 2010

[30] T. Ackermann. *Wind Power in Power Systems*. Chichester, UK: John Wiley & Sons, Ltd, 2005

[31] *Measurement and assessment of power quality characteristics of grid connected wind turbines*, IEC 61400-21, 2008

[32] P. Chirapongsananurak, and S. Santoso. "Harmonic analysis for fixed-speed wind turbines," *Power and Energy Society General Meeting (PES)*, pp. 1-4, July 21—25, 2013

[33] G. L. Xie, B. H. Zhang, Y. Li, and C. X. Mao. "Harmonic Propagation and Interaction Evaluation between Small-Scale Wind Farms and Nonlinear Loads," *Energies*, **6**, pp. 3297-3322, 2013

[34] K. Yang. *Wind-Turbine Harmonic Emissions and Propagation through A Wind Farm.* Degree: Licentiate of Engineering, Supervisor: Math H.J.Bollen, 2012

[35] *Testing and measurement techniques – Power quality measurement methods*. IEC standard 61000-4-30, 2008

[36] *General guide on harmonics and interharmonics measurements, for power supply systems and equipment connected thereto*. IEC standard 61000-4-7, 2009

[37] P. Ribeiro. *Time-Varying Waveform Distortions in Power Systems.* New Jersey: John Wiley & Sons, 2009

[38] G.W. Chang, and Cheng-I Chen. "Measurement Techniques for Stationary and Time-varying Harmonics," *IEEE Power & Energy Society General Meeting 2010*, pp. 1-5, Minneapolis, USA, July, 2010

[39] P.M. Silveira, C. Duque, T. Baldwin, and P.F. Ribeiro. "Sliding window recursive DFT with dyadic downsampling — A new strategy for time-varying power harmonic decomposition," *IEEE Power & Energy Society General Meeting*, 2009

[40] A. Bracale, P. Caramia, and G. Carpinelli. "Adaptive Prony Method for Waveform Distortion Detection in Power Systems," *Int. Journal of Electrical Power & Energy Systems*, **29**, 2007

[41] I. Gu, and M. H. J. Bollen. "Estimating Interharmonics by Using Sliding-Window ESPRIT," *IEEE Trans. on Pow. Del.*, **23**, 2008

[42] A. Bracale, G. Carpinelli, I. Y. H. Gu, and M. H.J. Bollen. "A new joint sliding-window ESPRIT and DFT scheme for waveform distortion assessment in power

systems," *Electric Power Systems Research*, **88**, pp. 112-120, 2012

[43] L. Alfieri, A. Bracale, P. Caramia, and G. Carpinelli. "Waveform Distortion Assessment in Power Systems with a New Three-step Sliding-Window Method," *13th Int. Conf. EEEIC*, Wroclaw, Poland, May 5—8, 2013

[44] J. Zygarlicki, M. Zygarlicka, J. Mroczka, K.J. Latawiec. "A Reduced Prony's Method in Power-Quality Analysis—Parameters Selection," *IEEE Transactions on Power Delivery*, **25**, pp. 979-986, 2010